A New Rectal Model for Dosimetry Applications

George Mardirossian, Magnus Tagesson, Pablo Blanco, Lionel G. Bouchet, Michael Stabin, Helio Yoriyaz, Souheil Baza, Michael Ljungberg, Sven-Erik Strand and A. Bertrand Brill

Department of Nuclear Medicine, University of Massachusetts Medical Center, Worcester, Massachusetts; Department of Radiation Physics, Lund University, Lund, Sweden; Department of Nuclear and Radiological Engineering, University of Florida, Gainesville, Florida; Medical Science Division, Oak Ridge Institute for Science and Education, Oak Ridge, Tennessee; Instituto de Pesquisas Energeticas e Nucleares, Sao Paulo, Brazil; and Faculty of Science, Aleppo University, Aleppo, Syria

A revised geometric representative model of the lower part of the colon, including the rectum, the urinary bladder and prostate, is proposed for use in the calculation of absorbed dose from injected radiopharmaceuticals. The lower segment of the sigmoid colon as described in the 1987 Oak Ridge National Laboratory mathematical phantoms does not accurately represent the combined urinary bladder/rectal/prostate geometry. In the revised model in this study, the lower part of the abdomen includes an explicitly defined rectum. The shape of sigmoid colon is more anatomically structured, and the diameters of the descending colon are modified to better approximate their true anatomic dimensions. To avoid organ overlap and for more accurate representation of the urinary bladder and the prostate gland (in the male), these organs are shifted from their originally defined positions. The insertion of the rectum and the shifting of the urinary bladder will not overlap with or displace the female phantom's ovaries or the uterus. In the adult male phantom, the prostatic urethra and seminal duct are also included explicitly in the model. The relevant structures are defined for the newborn and 1-, 5-, 10- and 15-y-old (adult female) and adult male phantoms. **Methods:** Values of the specific absorbed fractions and radionuclide S values were calculated with the SIMDOS dosimetry package. Results for ^{99m}Tc and other radionuclides are compared with previously reported values. **Results:** The new model was used to calculate S values that may be crucial to calculations of the effective dose equivalent. For ^{131}I, the S (prostate ← urinary bladder contents) and S (lower large intestine [LLI] wall ← urinary bladder contents) are 6.7×10^{-6} and 3.41×10^{-6} mGy/MBq × s, respectively. Corresponding values given by the MIRDOSE3 computer program are 6.23×10^{-6} and 1.53×10^{-6} mGy/MBq × s, respectively. The value of S (rectum wall ← urinary bladder contents) is 4.84×10^{-5} mGy/MBq × s. For ^{99m}Tc, we report S (testes ← prostate) and S (LLI wall ← prostate) of 9.41×10^{-7} and 1.53×10^{-7} mGy/MBq × s versus 1.33×10^{-6} and 7.57×10^{-6} mGy/MBq × s given by MIRDOSE3, respectively. The value of S (rectum wall ← prostate) for ^{99m}Tc is given as 4.05×10^{-6} mGy/MBq × s in the present model. **Conclusion:** The new revised rectal model describes an anatomically realistic lower abdomen region, thus giving improved estimates of absorbed dose. Due to shifting the prostate gland, a 30%–45% reduction in the testes dose and the insertion of the rectum leads to 48%–55% increase in the LLI wall dose when the prostate is the source organ.

Received Aug. 18, 1998; revision accepted Mar. 5, 1999.

For correspondence or reprints contact: George Mardirossian, PhD, University of Massachusetts Medical Center, Department of Nuclear Medicine, 55 Lake Ave. N., Worcester, MA 01655.

Key Words: Reference Man; human phantom; modeling; Monte Carlo simulation; S values

J Nucl Med 1999; 40:1524–1531

The close proximity of the prostate to the urinary bladder and the rectum, among other factors, imposes a limit on the absorbed dose that can be delivered safely to the prostate gland and tumor contained therein. In brachytherapy and external beam irradiation, this often leads to high exposure complications (*1–4*). For radioimmunoscintigraphy and other applications of internally distributed radionuclides, calculation of absorbed doses relies on standard models based on activity in source organs. Although three-dimensional, patient-specific, absorbed dose calculations are increasingly used for therapeutic radiopharmaceuticals, in which high-dose, nonstochastic effects may occur, standard anatomic models are generally adequate for radiation dosimetry of diagnostic radiopharmaceuticals, in which low-dose, stochastic radiation effects are of concern. The purpose of this study was to design a standard anatomic model that expresses a more valid representation of actual anatomy.

In the Oak Ridge National Laboratory (ORNL) Reference Man phantoms (*5–7*), the rectum was not included as a separate segment of the lower large intestine (LLI). The lower portion of the sigmoid colon did not adequately represent the rectum with distinct geometrical description (Fig. 1). In addition, the phantom shows the lower sigmoid segment diverting from the prostate (posterior view), and the lateral view (sagittal) reveals that the prostate (*8*) is approximately 1.5 cm from the outer wall of the anterior lower sigmoid colon.

Furthermore, because the rectum was not specifically simulated in the Reference Man phantom, doses received to the LLI from radioactivity in urinary bladder contents were often underestimated. This may hold true for ^{99m}Tc and other relatively short-lived agents (including antibody fragments) excreted intact through the kidneys or rapidly metabolized with urinary excretion of resulting catabolites.

The inclusion of the rectum as a specified segment to the LLI is desirable for many applications related to internal radiation dosimetry, including radioimmunotherapy, genito-

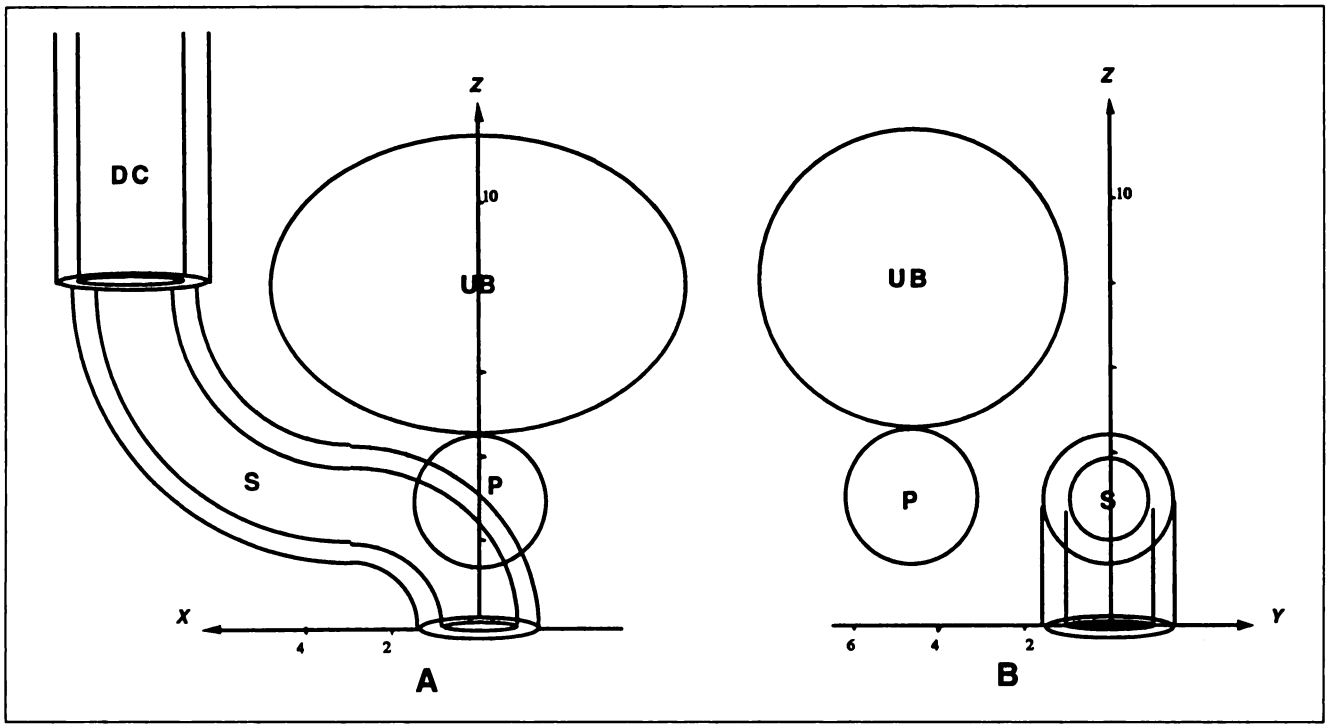

FIGURE 1. Lower abdomen region of adult male phantom as described by ORNL phantom representing posterior view (A) (observer in y-direction) and view from left lateral view (B) (observer in x-axis). All scales are in centimeters. DC = descending colon; P = prostate; S = sigmoid; UB = urinary bladder.

urinary and gastrointestinal (GI)-related studies. In this study, a rectum was added with appropriate geometry to the ORNL phantom(s), thus forcing a shift in the urinary bladder position and additional modifications to neighboring organs such as the prostate gland, sigmoid colon and descending colon. We therefore introduce the model and the mathematical organ's surface equations in defining organ volumes for convenient incorporation into Monte Carlo electron/photon transport codes, along with justifications for these geometrical changes to the mathematical representation of Reference Man. Additionally, postnatal phantoms as given by the ORNL reports, including the newborn and 1-, 5-, 10- and 15-y-old (adult female) phantoms, as well as the adult male phantom, were accordingly established and characterized.

MATERIALS AND METHODS

On the basis of anatomic descriptions (*9*) and information published by Cristy and Eckerman (*7*), a revision to the mathematical model of the ORNL adult male phantom is applied to the organs within the lower abdomen. The organs involved are the rectum, sigmoid colon, descending colon, prostate, urethra and urinary bladder, each in a manner described below.

Postnatal phantoms representing the newborn and 1-, 5-, 10- and 15-y-old (adult female) are also derived on the basis of physiological and anatomic descriptions given for Reference Man (*10*). Parameter values for the equations involved in describing anatomic structures and phantom variables are accordingly deduced. The defining equations were verified using numerical analysis and graphical methods on a personal computer using Microsoft Excel 5.0 spreadsheets (Microsoft, Redmond, WA). Furthermore, corrections for regional overlap during model development were made using Monte Carlo sampling techniques.

The Model

Anatomy. According to *Morris Human Anatomy* (*9*), the rectum begins at the third segment of the sacrum where the sigmoid mesocolon ceases (above the level of the urinary bladder). It extends caudally and, in general, ventrally after the slope of the corresponding portion of the sacrum and coccyx. In males, the fascial layer of the rectum is slightly fused with the fascia of the prostate gland, bladder and seminal vesicles. In females, there is a similar fascia where the rectum has contact with the vagina at the caudal portion of the rectum. Usually the rectum does not form a fecal reservoir. The feces are normally retained in the caudal part of the sigmoid colon, cranial to the first transverse fold, leaving the rectum empty except during defecation. The rectum ends at the junction with the anal canal, which turns sharply dorsally and caudally.

Mathematical Phantom. The sacrum in the ORNL adult male phantom (*7*) was included as part of the pelvic bone. In addition, the lower segment of the sigmoid colon ends at the x-y plane of the origin. Thus, the rectum wall in this model is simulated as the volume between two concentric right cylinders with its z central axis ending at the origin with a circular cross-section in the x-y plane (adult male, Fig. 2) and extending from the bottom of the trunk to the sigmoid colon. The sigmoid colon is interposed between the descending colon and the rectum. It is simulated as the volume between two semitori, representing an upper and a lower segment, with the outer wall diameters as described in earlier models (*5–7*) and equivalent to that of the new rectum model (Reference Man LLI diameter is 4 cm, and the rectum is 5 cm when empty; the sigmoid diameter in the ORNL phantom is 3.14 cm).

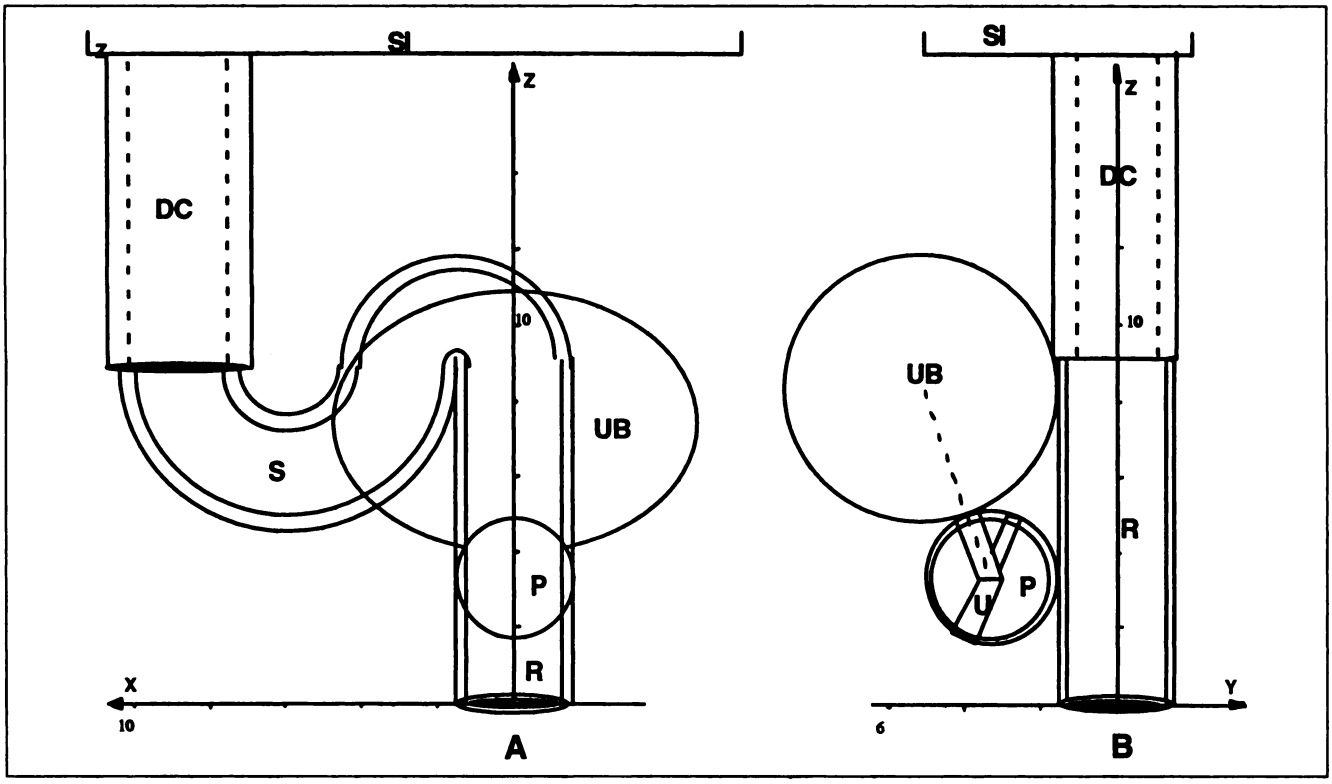

FIGURE 2. Rectal model is modification of lower abdomen region of ORNL phantom of Figure 1. Organs from posterior view (A) and from left lateral view (B). Small intestine (SI) remains unmodified in position (not shown in Figure 1). All scales are in centimeters. DC = descending colon; P = prostate; R = rectum; S = sigmoid; U = urethra; UB = urinary bladder.

The upper segment has a larger radius and forms with the lower segment an S-shaped structure at a 90° angle. This configuration allows the sigmoid colon to start and end at the same height (z-axis), so that the junction of the sigmoid colon and the rectum form a more or less acute angle (*9*).

According to International Commission on Radiological Protection (ICRP) Publication 23 (*10*), the total length of the LLI (all reference values refer to adult man) is 85 cm: 30 cm for the descending colon, 40 cm for the sigmoid colon and 15 cm for the rectum (Table 1). The length of the LLI in the ORNL/TM-8381 model, however, is only 29 cm (15.3 cm for the descending colon and 13.7 cm for the sigmoid colon) because the proper anatomic curvatures of the GI tract could not be mathematically modeled during the development of the original Medical Internal Radiation Dose (MIRD)-5-Revised phantom of Snyder et al. (*5*) and later by Cristy and Eckerman (*7*) in the ORNL phantom series. Because of its curvature, the large intestine is about three times shorter than the length recommended in ICRP Publication 23, and therefore model construction depended on matching masses (volumes) reference. In the model in this study, the sigmoid colon configuration allows the rectum to extend to the same z level at the end of the descending colon. This height in the adult male phantom is 8.72 cm and appears favorable for two reasons. First, because the anatomic rectum is less curved than the rest of the LLI, the ratio of the anatomic (12 cm) to the mathematical phantom (8.72 cm) lengths, 1.7, is proportionally representative. Second, with this configuration, the problem of avoiding anatomic overlaps with other tissue organs (such as the ovaries and uterus in the female phantom) becomes manageable.

TABLE 1
Comparison of Length and Weight for Lower Large Intestine (LLI) Segments in Adult Phantoms and Reference Man

	Length (cm)			Wall mass (g)		
Segment	ICRP 23*	ORNL	Present	ICRP 23*	ORNL	Present
Descending colon	25 (20–30)	15.3	15.3	90	93.5	89.8
Sigmoid colon	40 (12–84)	13.7†	13.3	50	73.3†	50.6
Rectum	15 (12–15)	—	8.7	20	—	19.8
Total LLI	85	29	37.3	160	166.8	160.2

*Reference Man values; numbers in parentheses represent range.
†Including rectum.

The ICRP Publication 23 (*10*) and Eve (*11*) give a mass for the adult LLI wall of 160 g (90, 50 and 20 g for the descending and sigmoid colons and the rectum, respectively) and a mass of the contents of 135 g. According to Eve, the feces accumulate principally in the sigmoid colon because of its horizontal portion. However, if the sigmoid colon happens to be full, the descending colon and part of the rectum will be filled. The presence of feces in the rectum will often lead to defecation, and therefore it is reasonable to assume an empty rectum in this model with a content medium equivalent to air (the feces medium is equivalent to soft tissue). Therefore, to conserve the LLI wall and content masses, the phantom relies on thickening the intestinal wall to match the anatomic Reference Man description. Likewise, we attempted to preserve the total mass of

all segments of the LLI. The thicknesses of the sigmoid and rectum were varied accordingly to match their anatomic values.

The length of the descending colon in the model in this study is the same as that in the ORNL phantom, but the semiaxis parameters, as well as the wall thickness, were allowed to change to conserve the total wall mass of 90 g and also the total content mass of 135 g within the LLI (exclusive of the rectum contents).

The rectal geometry and position as described above had forced a shifting of the urinary bladder, as defined in the ORNL phantom, anteriorly in the negative y direction to avoid region overlap (0.5 cm in the adult male phantom). This shifting enabled the prostate gland to be placed, as physically characterized by Stabin (*8*), between the rectum and urinary bladder walls in a more anatomically realistic location (Fig. 2B). A 1-mm-thick shell surrounding the prostate gland is included in the model to simulate a prostate capsule. This shell is in contact with both the rectal and urinary bladder walls. A prostatic urethra is also simulated in the adult male phantom. The prostatic urethra comprises the seminal duct and urinary bladder urethra and extends almost vertically caudally from the neck of the bladder. Both the seminal duct and the urinary bladder urethra segments are simulated as tilted cylinders with radii of 0.15 and 0.3 cm, respectively (Fig. 2B).

The wall masses and contents needed to construct the pediatric phantoms were produced in similar fashion as given by Christy and Eckerman (*7*). This procedure followed approximately the evolution of the trunk masses with subject age (*6,10*). The adult male organ masses (or organ parameters in the phantom) were used as normalization values from which the postnatal masses (parameters) were deduced. The descending colon semiaxes parameters in the pediatric phantoms were based on scaling downward the general semiaxis dimensions of the trunk. The two methods of scaling for the pediatric phantoms differ by a few percent. The final obtained semiaxis parameters for the GI tract were slightly adjusted to reach a compromise between the masses of both the walls and contents.

Rectum. The rectum is represented as two vertical elliptical and concentric cylinders that divide the organ into two parts: the wall and the contents. The wall is represented as the volume between the two external cylinders and is cut by two horizontal planes. The content is represented as the volume inside the internal surface of the wall. It is a vertical cylinder that begins with the descending sigmoid colon and ends at the anal opening at the axes origin. The general surface equations for the outer and inner rectal walls are defined by the following expressions:

$$\left(\frac{x}{a}\right)^2 + \left(\frac{y}{b}\right)^2 \le 1$$

$$\left(\frac{x}{a-d}\right)^2 + \left(\frac{y}{b-d}\right)^2 \le 1$$

$$0 \le z \le z_0.$$

The rectum's upper limit is equivalent to the lower limit of the descending colon and is 8.72 cm long for the Reference Man. The postnatal rectal lengths were also accordingly established. The rectum outer diameters are set as the outer diameters of the ORNL sigmoid colon. The adult male phantom thickness is set to correspond to the adult rectum mass of 15 g. Accordingly, the thickness of the rectal wall in the postnatal phantoms was adjusted in accordance to masses estimated in proportion to postnatal body weight growth with age. The calculated variables are presented in Table 2.

TABLE 2
Variables and Parameters of Rectum

Phantom	a	b	d	z_0	Volume (cm^3) Wall	Volume (cm^3) Content
Newborn	0.5	0.77	0.10	2.69	0.99	2.26
1 y	0.69	1.02	0.12	3.82	2.29	6.16
5 y	0.88	1.21	0.16	5.08	4.93	12.07
10 y	0.96	1.5	0.18	6.33	8.16	20.47
15 y*	1.18	1.76	0.22	7.86	14.78	36.51
Adult male	1.57	1.57	0.24	8.72	19.07	48.46

*Adult female.

Prostate. The prostate as originally defined by Stabin (*8*) is shown (Fig. 1B). In the model in this study, the prostate is shifted toward the positive y and positive z axes as described above. The radii of the prostate for various ages were derived from the mass of the postnatal prostate, as given in ICRP Publication 23 (*10*). In all cases, the prostate is surrounded by a 1-mm-thick shell. The spherical shape of the prostate satisfies the inequality:

$$x^2 + (y + y_0)^2 + (z - z_0)^2 \le a,$$

with variables defined by the values listed in Table 3.

Urethra. In this study, the prostatic urethra was only simulated in the adult male phantom. The prostatic urethra comprises the seminal duct (fed by the seminal vesicle, not simulated) and the urinary bladder urethra. The prostatic urethra is assumed flattened and simulated as a cylinder with a diameter of 0.6 cm. It extends through the prostatic capsule (shell) and may be described by the following inequality:

$$\left(\frac{x}{a}\right)^2 + \left(\frac{y - y_0}{b}\right)^2 \le 1. \qquad \text{Eq. 1}$$

The prostatic seminal duct enters from the posterior of the prostate gland traveling 1.09 cm toward the center before merging with the prostatic urethra. Its diameter is small and assumed to be half the diameter of the bladder urethra. This structure satisfies the following:

$$y_0 = 0.3797z - 4.4287 \qquad \text{Eq. 2}$$

$$3.65 \le z \le 4.743$$

$$a = 0.15, \quad b = 0.1605.$$

TABLE 3
Variables and Parameters of Prostate Gland

Phantom	y_0	z_0	a	Weight (g)	Volume (cm^3)
Newborn	1.45	0.844	0.58	0.82	0.817
1 y	1.72	1.552	0.6	0.9	0.905
5 y	1.97	2.235	0.66	1.2	1.204
10 y	2.32	2.987	0.72	1.6	1.563
15 y	2.86	3.586	1	4.3	4.189
Adult male	3.21	3.242	1.54*	14.93†	14.35†

*From reference 8.
†Excluding urethra weight and size.

TABLE 4
Variables and Parameters of Urinary Bladder

Phantom	a	b	c	d	y_0	z_0	Volume (cm^3) Wall	Content
Newborn	1.69	1.82	1.14	0.10	2.59	2.47	2.77	11.9
1 y	2.35	2.42	1.64	0.14	3.44	3.51	7.41	31.7
5 y	3.04	2.77	2.16	0.17	3.94	4.66	14.0	62.2
10 y	3.61	3.04	2.63	0.20	4.54	5.81	22.3	98.6
15 y*	4.27	3.38	3.11	0.23	5.14	7.21	34.5	154
Adult male	4.958	3.458	3.458	0.252	5.028	8.00	45.7	203

*Adult female.

The prostatic urethra moves almost from the top of the gland (connecting with the urinary bladder) toward the center, then diverts downward anteriorly outside the prostate. The simulation comprises two portions; the lower portion satisfies Equations 1 and 2 with the following boundaries:

$$1.677 \le z \le 3.21$$

$$a = 0.3, \quad b = 0.3209,$$

and the upper portion is described by Equation 1 and the following:

$$y_0 = -0.3797z - 1.9913$$

$$3.21 \le z \le 4.743$$

$$a = 0.3, \quad b = 0.3209.$$

Urinary Bladder. The urinary bladder, as indicated earlier, is shifted toward the y-axis in comparison with that in the ORNL phantom to accommodate the rectum without region overlap. Its wall thickness and diameters are otherwise unchanged:

$$\left(\frac{x}{a}\right)^2 + \left(\frac{y + y_0}{b}\right)^2 + \left(\frac{z - z_0}{c}\right)^2 \le 1$$

$$\left(\frac{x}{a - d}\right)^2 + \left(\frac{y + y_0}{b - d}\right)^2 + \left(\frac{z - z_0}{c - d}\right)^2 \ge 1,$$

where the variables for each phantom are defined in Table 4.

Descending Colon. The length of descending colon is the same as that of the ORNL phantom, but the semiaxis diameters are adjusted according to its anatomic values. It is still described as two coaxial elliptical cylinders with the cylinder axis at a slight angle with the z-axis of the phantom. The descending colon walls surface equations are defined as the following:

$$\left(\frac{x - x_0}{a}\right)^2 + \left(\frac{y - y_0}{b}\right)^2 \le 1$$

$$\left(\frac{x - x_0}{a - d}\right)^2 + \left(\frac{y - y_0}{b - d}\right)^2 \ge 1$$

$$x_0 = x_1 + \frac{m_x(z - z_2)}{z_2 - z_1}$$

$$y_0 = \frac{m_y(z_1 - z)}{z_2 - z_1}$$

$$z_1 \le z \le z_2,$$

with variables given in Table 5.

Sigmoid Colon. The sigmoid colon is defined as two semitori forming the upper and lower segments with circular axes and with outer cross-sections, as that described by Cristy and Eckerman (*7*). The wall thickness is adjusted to match the wall mass. The upper segment connects with the lower end of the descending colon, and the lower segment ends in connection with the rectum. The outer and inner walls are defined in the following equations for the upper and lower portions, respectively:

$$\left(\frac{\sqrt{(x - x_0)^2 + (z - z_0)^2} - R_1}{a}\right)^2 + \left(\frac{y}{b}\right)^2 \le 1$$

$$\left(\frac{\sqrt{(x - x_0)^2 + (z - z_0)^2} - R_1}{a - d}\right)^2 + \left(\frac{y}{b - d}\right)^2 \ge 1$$

$$z \le z_0$$

$$\left(\frac{\sqrt{(x - R_2)^2 + (z - z_0)^2} - R_2}{a}\right)^2 + \left(\frac{y}{b}\right)^2 \le 1$$

$$\left(\frac{\sqrt{(x - R_2)^2 + (z - z_0)^2} - R_2}{a - d}\right)^2 + \left(\frac{y}{b - d}\right)^2 \ge 1$$

$$z \ge z_0,$$

TABLE 5
Variables and Parameters of Descending Colon

Phantom	a	b	d	x_1	m_x	m_y	z_1	z_2	Volume (cm^3) Wall	Contents
Newborn	0.55	0.95	0.21	2.94	0.2477	1.225	2.69	7.41	4.02	3.73
1 y	0.77	1.26	0.29	4.07	0.3432	1.625	3.82	10.53	10.64	9.81
5 y	1.00	1.46	0.37	5.30	0.4466	1.875	5.08	13.99	21.65	19.22
10 y	1.21	1.63	0.44	6.43	0.5421	2.10	6.33	17.42	36.79	31.92
15 y*	1.51	1.92	0.52	7.98	0.6728	2.45	7.86	21.63	66.49	58.93
Adult male	1.74	1.94	0.58	9.25	0.78	2.5	8.72	24	86.31	75.73

*Adult female.

TABLE 6
Variables and Parameters of Sigmoid Colon

Phantom	a	b	d	x_0	z_0	R_1	R_2	Volume (cm^3) Wall	Volume (cm^3) Contents
Newborn	0.5	0.77	0.16	1.84615	2.69	0.84615	0.5	2.360	2.756
1 y	0.69	1.02	0.22	2.5534	3.82	1.1734	0.69	6.029	6.915
5 y	0.88	1.21	0.28	3.3067	5.08	1.5467	0.88	12.138	13.364
10 y	0.96	1.50	0.34	3.90395	6.33	1.98395	0.96	20.943	20.897
15 y*	1.18	1.76	0.41	4.8336	7.86	2.4736	1.18	37.405	37.484
Adult male	1.57	1.57	0.43	5.805	8.72	2.665	1.57	48.707	54.320

*Adult female.

with parameters as given in Table 6. To avoid geometrical aberrations, the exact values of R_1 and x_0 given in Table 6 may be obtained from the following:

$$R_1 = \frac{(x_1 - m_x)_{TABLE\,5}}{2} - R_2$$

$$x_0 = (x_1 - m_x)_{TABLE\,5} - R_1.$$

Calculation Methods. We used the Monte Carlo code SIMDOS (*12*) to determine S values obtained after the inclusion of this new model into the ORNL phantom. Briefly, this code has the ability to perform radiation transport in arbitrary mathematical phantoms as well as in voxel-based phantoms. Simulation of photons and electrons (including full β spectra when needed) transported in various media may be performed in the described model. In this study, sampling of decay sites was performed in each source region. The decay scheme data used in SIMDOS is taken from ICRP Publication 38 (*13*) with β components taken from Simpkin and Mackie (*14*). Both photons and electrons were followed in their tracks throughout the calculation based on probability of interaction and hence transported until they either escape the phantom geometry or drop in energy to a level below a cutoff energy predefined at 4 keV for photons and 12 keV for electrons. Particles with energies below the cutoff are then considered locally absorbed. A total of 40,000 radionuclide decays representing ^{131}I, ^{111}In and ^{99m}Tc were simulated to obtain S values used in the comparison with both Stabin (*8*) and MIRDOSE3 (*15*) results.

RESULTS

Because of the new configuration of the LLI presented in this study, wall masses in each segment were maintained according to Reference Man guidance as well as the mass of the LLI content. The mass results obtained in this study are compared with the ORNL phantom values in Table 7, which show some minor variations among larger phantoms variables. This is due to the original work of Cristy (*6*), in which the "soft tissue" density value was considered 0.9869 g/cm^3 and later changed to 1.04 g/cm^3 without changing the model parameters (*7*). This arrangement is not at all considered serious in the framework of the Reference Man variations, but we sought to normalize the masses in this study because a new set of parameters was established. The parameters derived in this study were based on Reference Man LLI wall and content mass values of 160 and 135 g, respectively (*10*). Table 8 compares S values obtained in this study with Stabin (*8*) or MIRDOSE3 software (*13*) results for ^{99m}Tc, ^{111}In and ^{131}I radionuclides, when the prostate gland or the urinary bladder is homogeneously filled as a source organ. The S values were derived from the adult male phantom and included (in parenthesis) the percent relative errors recorded for each S value. In this table, the prostate was assumed not to include the prostatic urethra and seminal duct, i.e., the prostate volume is the sphere excluding the volumes defined by the prostatic urethra and seminal duct.

DISCUSSION

The ORNL phantoms and Reference Man are landmark developments embedded in much of the radiation dosimetry methods in current use. New phantoms representing different pre- and postnatal ages have been developed, and these add to the reliability of calculations that can be made for individuals of different status. As one develops new phantom geometries for specialized purposes, as we have done for prostate dose estimation, one changes organ features (organ mass and location) in the altered regions that would

TABLE 7
Comparison Between Lower Large Intestine Properties as Obtained in Present and Cristy/Eckerman Models

Phantom	Rectal model Length (cm)	Rectal model Wall (g)	Rectal model Contents* (g)	Cristy/Eckerman Length (cm)	Cristy/Eckerman Wall (g)	Cristy/Eckerman Contents* (g)
Newborn	11.6	7.7	6.7	9.0	7.8	6.8
1 y	16.4	19.7	17.4	12.7	20.6	18.3
5 y	21.6	40.3	33.9	16.9	41.5	36.6
10 y	26.7	68.5	54.9	21.0	70.0	61.8
15 y†	33.1	123.4	100.3	26.1	127.0	109.2
Adult male	37.3	160.2‡	135.3§	29.0	166.8‡	143.1§

*Excluding rectum content.
†Adult female.
‡Reference man (ICRP 23) value 160 g.
§Reference man (ICRP 23) value 135 g.

TABLE 8
Comparison of S Values (mGy/MBq × s) for ^{99m}Tc, ^{111}In and ^{131}I with Source Organ in Prostate and Urinary Bladder Contents

	Prostate									Urinary bladder content								
	^{99m}Tc			^{111}In			^{131}I			^{99m}Tc			^{111}In			^{131}I		
Target region	Stabin*	This model	Diff. (%)	Stabin*	This model	Diff. (%)	Stabin*	This model	Diff. (%)	MIRDOSE3	This model	Diff. (%)	MIRDOSE3	This model	Diff. (%)	MIRDOSE3	This model	Diff. (%)
Prostate gland	2.11E-04	2.37E-04 (0.2)	11	5.54E-04	5.78E-04 (0.3)	4	2.04E-03	2.14E-03 (0.1)	5	2.27E-06†	2.03E-06 (5.9)	−12	2.27E-06†	2.03E-06 (5.9)	−12	2.27E-06†	2.03E-06 (5.9)	−12
Urinary bladder wall	2.50E-06	2.28E-06 (4.0)	−10	7.22E-06	7.97E-06 (2.0)	9	6.94E-06	6.95E-06 (4.7)	0.1	1.14E-05	1.18E-05 (0.3)	3	1.14E-05	1.18E-05 (0.3)	3	1.14E-05	1.18E-05 (0.3)	3
Testes	1.33E-06	9.41E-07 (6.3)	−41	4.12E-06	2.85E-06 (4.7)	−45	3.65E-06	2.78E-06 (8.8)	−31	3.72E-07	3.00E-07 (13)	−24	3.72E-07	3.00E-07 (13)	−24	3.72E-07	3.00E-07 (13)	−24
Lower large intestine wall	7.57E-07	1.53E-06 (6.3)	51	2.34E-06	5.08E-06 (4.9)	54	2.09E-06	4.42E-06 (8.1)	53	5.77E-07	1.10E-06 (6.6)	48	5.77E-07	1.10E-06 (6.6)	48	5.77E-07	1.10E-06 (6.6)	48
Rectum wall	—	4.05E-06 (4.7)	—	—	1.41E-05 (2.1)	—	—	1.15E-05 (4.0)	—	—	1.33E-06 (8.4)	—	—	1.33E-06 (8.4)	—	—	1.33E-06 (8.4)	—
Prostatic urethra	—	4.37E-05 (5.2)	—	—	1.77E-04 (3.2)	—	—	2.50E-04 (4.8)	—	—	1.78E-06 (27)	—	—	1.78E-06 (27)	—	—	1.78E-06 (27)	—
Prostatic seminal duct	—	4.46E-05 (18)	—	—	2.19E-04 (6.3)	—	—	3.82E-04 (7.5)	—	—	4.27E-06 (49)	—	—	4.27E-06 (49)	—	—	4.27E-06 (49)	—

*Reference 8.
†Reference 8, S (urinary bladder ← prostate gland), by reciprocity.
Diff. = difference.
Percent relative errors are in parentheses.

result in different organ dose estimates if used for general purpose calculations. In this model, we have included an explicitly defined rectum modeled as a vertical cylinder starting at the anal opening (axis origin) and with outer diameters similar to the sigmoid colon being (a) part of the LLI and (b) geometrically representative of Reference Man values. The sigmoid colon was accordingly reshaped to accommodate the new rectum and to simulate its true anatomic geometry and curvature. Because the intestinal tract and curvatures are not mathematically presentable, we relied on thickening the wall to preserve anatomic wall mass and content mass. To accommodate the new rectum without overlapping other organs, the urinary bladder was also shifted in the adult male phantom approximately 0.5 cm anteriorly (less for other aged phantoms). The prostate with its 1-mm-thick shell capsule accommodated the space between the rectum and the bladder walls, simulating its true anatomic position. The ORNL total lengths of the LLI are presented in Table 7, along with the computed masses for that geometry and the values listed in Reference Man. Discrepancies in mass are small, but because of configurational variations, there may be significant differences in dose from systemically injected radiopharmaceuticals.

As an illustration of the new model, S values were calculated for radioactivity of ^{99m}Tc, ^{111}In and ^{131}I in the prostate gland or the urinary bladder (Table 8). Because target organs are sampled at close proximity to the source organ, only 50,000 decays were generated in the Monte Carlo SIMDOS code. The percent relative errors reported in Table 8 are considered to statistically satisfy the purpose of this calculation. Small organs such as the prostatic urethra and the prostatic seminal duct reflected much larger errors due to lesser histories recorded therein. The results are approximately 10%–15% different in the present calculation in comparison with ORNL's phantom geometry, which basically reflects variations between the two calculation platforms. The estimated dose to the testes, however, reveals reduction in the present estimation by approximately 30%–45% when the prostate presents the source organ. This is because the prostate gland is being moved posteriorly in the present model. The S (LLI wall ← prostate gland) and S (LLI wall ← urinary bladder contents) values show significant increases compared with the ORNL model values. The increase, ranging from 48% to 55%, is fully explained by the closer vicinity between the prostate and urinary bladder and the LLI with the new model.

CONCLUSION

The rectal model we have proposed revises the geometry for the lower part of the large intestine and provides a more anatomically realistic model for the relationships among structures in this region. Calculations using these revised coordinates should provide more accurate estimates of absorbed doses to the urinary bladder, prostate, urethra and rectum wall from injected diagnostic and therapeutic radiopharmaceuticals. Accuracy is particularly important for treatment planning in radiation therapy protocols, in which it is important to estimate the dose to nearby healthy organs. Ideally, one will do patient-specific dose calculations for treating a given patient, but general guidance including a comparison of doses from different radiopharmaceuticals can be assessed from standard phantom calculations, and the revised phantom geometry for the rectal region may be of use for this purpose.

ACKNOWLEDGMENTS

The authors thank Dr. Wesley Bolch, of the University of Florida at Gainesville, for his guidance and positive comments during the preparation of this study. This work was partially supported by grants from the Swedish Radiation Protection Institute #1009.97.

REFERENCES

1. Fuks Z, Leibel SA, Wallner KE, et al. The impact of local control on metastatic dissemination in carcinoma of the prostate: long-term in patients treated with 125-iodine implantation. *Int J Radiat Oncol Biol Phys.* 1991;21:537–547.
2. Hanks GE. External beam radiation therapy for clinically localized prostate cancer: pattern of care studies in the United States. *Natl Cancer Inst Monograph.* 1988;7:75–84.
3. Marinelli D, Shanberg AM, Tanzey LA, Sawyer DE, Syed N, Puthawala A. Follow-up prostate biopsy in patients with carcinoma of the prostate treated by 192-iridium template irradiation plus supplemental external beam radiation. *J Urol.* 1992;147:922–925.
4. Benk VA, Adams JA, Shipley WU, et al. Late rectal bleeding following x-ray and proton high dose irradiation for patients with stages T3-T4 prostatic carcinoma. *Int J Radiat Oncol Biol Phys.* 1993;26:551–557.
5. Snyder WS, Ford MR, Warner GG, Watson SB. *A Tabulation of Dose Equivalent per Microcurie-day for Source and Target Organs of an Adult for Various Radionuclides: part 1.* Oak Ridge National Laboratory Report ORNL-5000. Oak Ridge, TN: Oak Ridge National Laboratory; 1974.
6. Cristy M. *Mathematical Phantoms Representing Children of Various Ages for Use in Estimates of Internal Dose.* Oak Ridge National Laboratory Report ORNL/NUREG/TM-367. Oak Ridge, TN: Oak Ridge National Laboratory; 1980.
7. Cristy M, Eckerman KF. *Specific Absorbed Fractions of Energy at Various Ages from Internal Photon Sources. I. Methods.* Oak Ridge National Laboratory Report ORNL/TM-8381/V1. Oak Ridge, TN: Oak Ridge National Laboratory; 1987.
8. Stabin M. A model for the prostate gland for internal dosimetry. *J Nucl Med.* 1994;35:516–520.
9. Anson Barry J. *Morris Human Anatomy.* 12th ed. New York, NY: McGraw-Hill Book Co., 1966:1334–1335.
10. International Commission on Radiological Protection. *Report of the Task Group on Reference Man.* ICRP publication 23. Oxford, UK: Pergamon Press; 1976.
11. Eve IS. A review of the physiology of the gastrointestinal tract in relation to radiation doses from radioactive materials. *Health Phys.* 1966;12:131–161.
12. Tagesson M, Ljungberg M, Strand SE. A Monte Carlo program converting activity distributions to absorbed dose distributions in a radionuclide treatment planning system. *Acta Oncol.* 1996;35:367–372.
13. Snyder WS, Fors MR, Bernard SR, et al. *Radionuclide Transformations, Energy and Intensity of Emissions.* ICRP publication 38. New York, NY: Pergamon Press; 1983.
14. Simpkin DJ, Mackie TR. EGS4 Monte Carlo determination of the beta dose kernel in water. *Med Phys.* 1990;17:179–186.
15. Stabin M. MIRDOSE: the personal computer software for use in internal dose assessment in nuclear medicine. *J Nucl Med.* 1996;37:538–546.